


Asymmetric Elastic Metasurface for Wave Manipulation Between Different Media

Sang Vin Jang¹, Sung Won Lee¹, and Joo Hwan Oh^{1*}

School of Mechanical Engineering, Ulsan National Institute of Science and Technology, UNIST-gil 50, Eonyang-eup, Ulju-gun, Ulsan, 44919, South Korea

 (Received 11 October 2022; revised 8 December 2022; accepted 23 December 2022; published 13 February 2023)

This paper mainly studies the problem of metasurfaces between different mediums. Despite recent advances on metasurfaces, there has been a critical limitation that wave manipulation between two different mediums is theoretically impossible with general approaches since full transmission and desired phase shift cannot be achieved simultaneously. In order to get over this theoretical issue, we propose an asymmetric metasurface that can manipulate waves between two different mediums. By introducing the asymmetry, achieving both full transmission and desired phase shift simultaneously is theoretically enabled. From theoretical approaches, an actual continuum metasurface is designed and applied to various wave manipulations between two different mediums. We expect that the proposed metasurface can be applied to various applications in the area of ultrasonics and vibrations.

DOI: [10.1103/PhysRevApplied.19.024036](https://doi.org/10.1103/PhysRevApplied.19.024036)

I. INTRODUCTION

Recently, wave physics has been largely broadened by metamaterials, artificial materials consisting of subwavelength unit cells, owing to their various extraordinary wave characteristics such as negative parameters or refractive index. However, metamaterials have a critical drawback in that a large size is required due to periodicities. To overcome this limitation, metasurfaces have attracted much attention in various fields such as electromagnetics [1–6], acoustics [7–11], and elasticity [12–20]. A metasurface is a thin surface consisting of subwavelength unit cells, in which the unit cells are designed to provide proper phase shifts with zero reflection. By arranging unit cells with the desired phase shifts, the metasurface enables wave manipulation based on the generalized Snell's law [1]. In fact, metasurfaces have successfully manipulated reflected [8,10,11,13] or refracted [5,7,12,15,16,19,20] waves to achieve various wave phenomena such as focusing [2,6,14,17,18], cloaking [4,9], and holography [3,11]. Since various wave manipulations are possible with a thin surface, metasurfaces are expected to break through various limitations and enrich the current knowledge of wave physics.

However, despite active research, previous attempts with acoustic or elastic metasurfaces have mainly focused on the homogeneous case where a metasurface is installed between the same wave medium. Recently, Lee *et al.* [19] reported that if a metasurface were to be located between

different wave mediums, the previous studies could not be applied at all. In general, to achieve wave manipulation with a metasurface, each metasurface unit should be designed to satisfy two conditions: full transmission and the desired phase shift. This has been well achieved in the homogeneous case. However, Lee *et al.* [19] showed that for the inhomogeneous case where there are different wave mediums on each side of the metasurface, the two conditions are coupled so that they cannot be satisfied simultaneously in general. Thus, wave manipulation between two different mediums is impossible. Because of this limitation, Lee *et al.* [19] combined two types of metasurface to tailor waves between two different mediums: one as the phase shifter and the other as the impedance matcher. Unfortunately, this was not a clear solution for the inhomogeneous case, and there has still been no research solving this challenge. Furthermore, most applications in elastic waves involve multiple mediums [21–23], indicating that this challenge is not only scientifically interesting but also practically important to enable various innovations.

In this work, we propose a single-unit asymmetric metasurface that solves the challenge and manipulates waves between two different mediums. The key idea of this work is asymmetry. In general, unit cells of the metasurface are modeled as a mass-spring system, as shown in Fig. 1(a), that connects two neighboring mediums. Previously, the left and right equivalent springs were set to be identical for simplicity. However, such a symmetric system could not achieve both full transmission and the desired phase shift, which are essential in wave manipulation by metasurfaces. Here, we find that if the equivalent springs are different on the left and right, as in Fig. 1(b), the full transmission

*joo-hwan.oh@unist.ac.kr

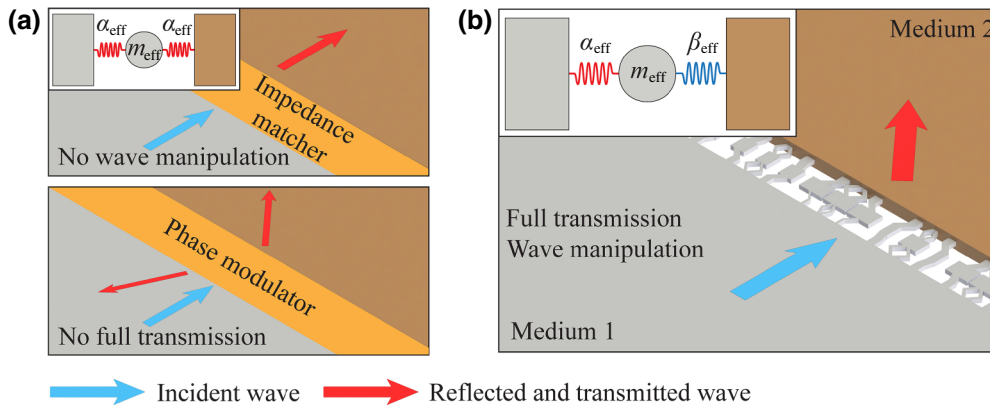


FIG. 1. The schematics of (a) the previous symmetric metasurface and (b) the proposed asymmetric metasurface between two different mediums.

condition and the desired phase shifts are decoupled so that the two conditions can be satisfied simultaneously. Thus, by arranging the asymmetric unit cells with the desired phase shift, it is now possible to achieve wave manipulation between two different mediums, which was previously only achievable with double-unit metasurfaces [19].

To validate our idea of an asymmetric metasurface, actual metasurface unit cells are designed and wave manipulation between two different mediums is numerically studied. To this end, we adopt the previously proposed single-unit metasurface [19,20], which has been successfully used to manipulate waves in a single-medium case but could not be used between two different mediums due to its symmetric configuration. Here, we extend the single-unit metasurface to have the asymmetry so that it can be applied between two different mediums. Theoretical investigations are made to show the equivalence between the proposed single-unit asymmetric metasurface and the asymmetric mass-spring system in Fig. 1(b). After the theoretical investigation, the actual asymmetric unit cell is designed by the optimization method. With the designed unit cells, wave simulations are carried out to validate that both full transmission and the desired phase shifts are simultaneously achieved by the idea of asymmetry. Finally, the feasibility of wave manipulation between two different mediums is shown with various numerical supports such as wave refraction, mode coupling, and wave focusing between two different mediums.

This paper is organized as follows. First, the theoretical background of the existing symmetric metasurface is introduced to show the single-unit symmetric system cannot achieve wave manipulation under full transmission. Then, it is analytically shown that the asymmetric mass-spring system can satisfy both objectives. After that, the relation between the asymmetric system and the equivalent system is derived. Based on the relationship between them, the actual system is designed by optimizing the design parameters. Finally, the designed units and metasurface are validated through numerical analysis. In addition to the results, various applications using the proposed metasurface are introduced.

II. THEORETICAL BACKGROUND OF ASYMMETRIC METASURFACES

Prior to introducing the proposed asymmetric idea, it is worth reviewing why symmetric metasurfaces have limitations [19]. In wave manipulation by metasurfaces, it is essential to achieve unit cells with both full transmission and the desired phase shifts. However, previous symmetric metasurfaces could not achieve both conditions simultaneously so that they could not be applied to the wave manipulation between two different mediums. We explain why the symmetric metasurfaces cannot achieve both conditions. In addition, the idea of the asymmetric metasurface is theoretically explained.

A. Theoretical limitation of symmetric metasurfaces

Figure 2 plots the mass-spring system of the symmetric metasurface between two different mediums. Here, the longitudinal wave is considered. For theoretical investigation, incident, reflected, and transmitted waves are described with the transfer matrix [24,25]. Considering the physics at the left and right boundaries of the mediums, the displacement and force at the boundaries are written as, for $x \leq 0$,

$$u = (A_1 e^{-ik_1 x} + B_1 e^{ik_1 x}) e^{i\omega t}, \quad (1)$$

$$f = (-i\omega Z_1 A_1 e^{-ik_1 x} + i\omega Z_1 B_1 e^{ik_1 x}) e^{i\omega t}, \quad (2)$$

and for $x \geq d$,

$$u = A_2 e^{-ik_2(x-d)} e^{i\omega t}, \quad (3)$$

$$f = -i\omega Z_2 A_2 e^{-ik_2(x-d)} e^{i\omega t}. \quad (4)$$

Here, the time-harmonic assumption is applied, so displacements are described with angular frequency ω and time t . A_1 , B_1 , and A_2 are the amplitudes of displacement for each incident, reflected, and transmitted wave respectively. Since wave mediums at $x = 0$ and $x = d$ are different, the impedance Z and wave number k are independently defined, denoted by the subscripts 1 and 2,

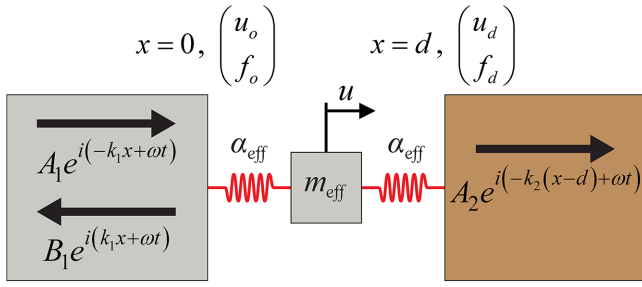


FIG. 2. Symmetric mass-spring system between two different mediums.

respectively. It is worth noting that the force at each boundary is obtained from the concept of mechanical impedance $f = Z \partial u / \partial t$. From these expressions, the displacement and force at the boundaries $x = 0$ and $x = d$ are expressed in matrix form as

$$\begin{pmatrix} u_o \\ f_o \end{pmatrix} = \mathbf{M}_1 \begin{pmatrix} A_1 \\ B_1 \end{pmatrix} e^{i\omega t}, \quad \begin{pmatrix} u_d \\ f_d \end{pmatrix} = \mathbf{M}_2 \begin{pmatrix} A_2 \\ 0 \end{pmatrix} e^{i\omega t}, \quad (5)$$

where

$$\mathbf{M}_n = \begin{pmatrix} 1 & 1 \\ -i\omega Z_n & i\omega Z_n \end{pmatrix}. \quad (6)$$

Now, let us focus on the mass-spring system connecting the two boundaries. From the mass-spring system, the following equations can be derived using the effective mass m_{eff} and the effective spring coefficient α_{eff} :

$$\begin{aligned} -\omega^2 m_{\text{eff}} u &= \alpha_{\text{eff}}(u_o + u_d - 2u), \\ f_o &= \alpha_{\text{eff}}(u_o - u), \\ f_d &= \alpha_{\text{eff}}(u - u_d). \end{aligned} \quad (7)$$

These equations can be summarized as

$$u_d = \frac{\alpha_{\text{eff}} - \omega^2 m_{\text{eff}}}{\alpha_{\text{eff}}} u_o + \frac{2\alpha_{\text{eff}} - \omega^2 m_{\text{eff}}}{\alpha_{\text{eff}}^2} f_o, \quad (8)$$

$$f_d = -\omega^2 m_{\text{eff}} u_o + \frac{\alpha_{\text{eff}} - \omega^2 m_{\text{eff}}}{\alpha_{\text{eff}}} f_o, \quad (9)$$

or, in the matrix form,

$$\begin{pmatrix} u_d \\ f_d \end{pmatrix} = \mathbf{T} \begin{pmatrix} u_o \\ f_o \end{pmatrix},$$

$$\mathbf{T} = \begin{pmatrix} T_{11} & T_{12} \\ T_{21} & T_{22} \end{pmatrix} = \begin{pmatrix} \frac{\alpha_{\text{eff}} - \omega^2 m_{\text{eff}}}{\alpha_{\text{eff}}} & \frac{2\alpha_{\text{eff}} - \omega^2 m_{\text{eff}}}{\alpha_{\text{eff}}^2} \\ -\omega^2 m_{\text{eff}} & \frac{\alpha_{\text{eff}} - \omega^2 m_{\text{eff}}}{\alpha_{\text{eff}}} \end{pmatrix}. \quad (10)$$

Finally, substituting Eqs. (5) and (6) into Eq. (10), the relation among the amplitudes of displacement can be

described,

$$\begin{pmatrix} A_2 \\ 0 \end{pmatrix} = \mathbf{M}_2^{-1} \mathbf{T} \mathbf{M}_1 \begin{pmatrix} A_1 \\ B_1 \end{pmatrix} = \mathbf{S} \begin{pmatrix} A_1 \\ B_1 \end{pmatrix}. \quad (11)$$

Equation (11) can be rewritten by using the inverse matrix, \mathbf{S}^{-1} ,

$$\begin{pmatrix} A_1 \\ B_1 \end{pmatrix} = \mathbf{S}^{-1} \begin{pmatrix} A_2 \\ 0 \end{pmatrix}. \quad (12)$$

From Eq. (12), the transmission and reflection coefficients are derived as

$$T = \frac{A_2}{A_1} = \frac{2i\omega Z_1}{T_{21} - \omega^2 Z_1 Z_2 T_{12} + i\omega(Z_2 + Z_1)T_{11}}, \quad (13)$$

$$R = \frac{B_1}{A_1} = -\frac{T_{21} + \omega^2 Z_1 Z_2 T_{12} + i\omega(Z_2 - Z_1)T_{11}}{T_{21} - \omega^2 Z_1 Z_2 T_{12} + i\omega(Z_2 + Z_1)T_{11}}. \quad (14)$$

In the full transmission condition, the incident wave energy should be fully transmitted. In other words, the reflected energy should be equal to zero, so the magnitude of the reflection coefficient should be also zero. From Eq. (14), the magnitude can be derived as

$$|R| = \sqrt{\frac{(T_{21} + \omega^2 Z_1 Z_2 T_{12})^2 + \omega^2 (Z_2 - Z_1)^2 T_{11}^2}{(T_{21} - \omega^2 Z_1 Z_2 T_{12})^2 + \omega^2 (Z_2 + Z_1)^2 T_{11}^2}}. \quad (15)$$

Previously, the metasurface was inserted between same medium so that $Z_1 = Z_2$. However, in this case, the wave medium is not same so that $Z_2 - Z_1$ is nonzero. Accordingly, the full transmission condition is expressed as

$$T_{11} = 0, \quad T_{21} + \omega^2 Z_1 Z_2 T_{12} = 0. \quad (16)$$

Substituting the elements of the transfer matrix from Eq. (10) into the full transmission conditions Eq. (16), the following relations are derived [19]:

$$m_{\text{eff}} = \sqrt{Z_1 Z_2} / \omega, \quad \alpha_{\text{eff}} = \omega \sqrt{Z_1 Z_2}. \quad (17)$$

Again, substituting Eqs. (10) and (17) into Eq. (13), the transmission coefficient can be rewritten as [19]

$$T = \mp i \sqrt{\frac{Z_1}{Z_2}}. \quad (18)$$

Equation (18) indicates that the transmission coefficient is always purely imaginary if full transmission is achieved. In other words, under full transmission, only the phase shifts of $\pi/2$ or $3\pi/2$ are possible, and to achieve other phase shifts, full transmission should be abandoned. Since both full transmission and various phase shifts are essential to manipulate waves with metasurfaces, Eq. (18) clearly

shows that it is impossible to manipulate waves between two different mediums with the previously considered metasurfaces.

Note that in Eq. (18), although the reflection is zero, the magnitude of the transmission coefficient, $|T|$, is not equal to 1. This is because the transmission coefficient is defined by the ratio of the amplitude, not by the wave energy. Since the wave mediums are different, the wave amplitudes are also different for some amount of the energy, resulting in the transmission coefficient being different from 1.

B. Asymmetric mass-spring system

Previously, it was shown that wave manipulation between two different mediums is impossible with the previously studied symmetric metasurfaces. In this section, the asymmetric mass-spring system that can overcome the limitation is theoretically studied. Figure 3 plots the asymmetric mass-spring system that has effective spring coefficients α_{eff} and β_{eff} to connect two different mediums. As in the previous approach, the transfer matrix is derived. From the equation of motion, the displacement and force at the boundary $x = d$ are expressed as

$$m_{\text{eff}} \frac{\partial^2 u}{\partial t^2} = \alpha_{\text{eff}}(u_o - u) + \beta_{\text{eff}}(u_d - u), \quad (19)$$

$$u_d = \frac{\beta_{\text{eff}} - \omega^2 m_{\text{eff}}}{\beta_{\text{eff}}} u_o + \frac{\alpha_{\text{eff}} + \beta_{\text{eff}} - \omega^2 m_{\text{eff}}}{\alpha_{\text{eff}} \beta_{\text{eff}}} f_o, \quad (20)$$

$$f_d = -\omega^2 m_{\text{eff}} u_o + \frac{\alpha_{\text{eff}} - \omega^2 m_{\text{eff}}}{\alpha_{\text{eff}}} f_o. \quad (21)$$

Then, the transfer matrix for the asymmetric system can be derived as

$$\begin{pmatrix} u_d \\ f_d \end{pmatrix} = \begin{pmatrix} \frac{\beta_{\text{eff}} - \omega^2 m_{\text{eff}}}{\beta_{\text{eff}}} & \frac{\alpha_{\text{eff}} + \beta_{\text{eff}} - \omega^2 m_{\text{eff}}}{\alpha_{\text{eff}} \beta_{\text{eff}}} \\ -\omega^2 m_{\text{eff}} & \frac{\alpha_{\text{eff}} - \omega^2 m_{\text{eff}}}{\alpha_{\text{eff}}} \end{pmatrix} \times \begin{pmatrix} u_o \\ f_o \end{pmatrix} = \mathbf{T}^* \begin{pmatrix} u_o \\ f_o \end{pmatrix}, \quad (22)$$

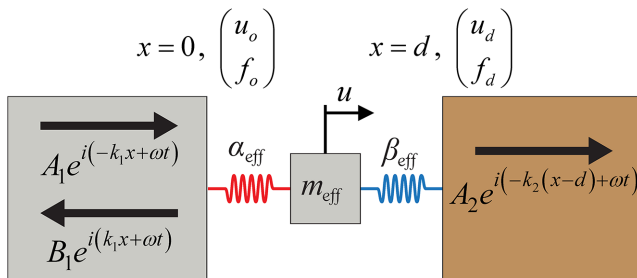


FIG. 3. Asymmetric mass-spring system between two different mediums.

$$\mathbf{T}^* = \begin{pmatrix} \frac{\beta_{\text{eff}} - \omega^2 m_{\text{eff}}}{\beta_{\text{eff}}} & \frac{\alpha_{\text{eff}} + \beta_{\text{eff}} - \omega^2 m_{\text{eff}}}{\alpha_{\text{eff}} \beta_{\text{eff}}} \\ -\omega^2 m_{\text{eff}} & \frac{\alpha_{\text{eff}} - \omega^2 m_{\text{eff}}}{\alpha_{\text{eff}}} \end{pmatrix}. \quad (23)$$

Comparing Eq. (23) with the transfer matrix of the symmetric system in Eq. (10), one can clearly observe that the diagonal terms T_{11}^* and T_{22}^* are no longer the same due to the asymmetry. Accordingly, the transmission and reflection coefficients are derived differently as

$$T = \frac{A_2}{A_1} = \frac{2i\omega Z_1}{T_{21}^* - \omega^2 Z_1 Z_2 T_{12}^* + i\omega(Z_2 T_{11}^* + Z_1 T_{22}^*)}, \quad (24)$$

$$R = \frac{B_1}{A_1} = -\frac{T_{21}^* + \omega^2 Z_1 Z_2 T_{12}^* + i\omega(Z_2 T_{11}^* - Z_1 T_{22}^*)}{T_{21}^* - \omega^2 Z_1 Z_2 T_{12}^* + i\omega(Z_2 T_{11}^* + Z_1 T_{22}^*)}. \quad (25)$$

From Eq. (25), the full transmission condition can be derived by considering the zero-reflection case, as

$$|R| = \frac{\sqrt{(T_{21}^* + \omega^2 Z_1 Z_2 T_{12}^*)^2 + \omega^2 (Z_2 T_{11}^* - Z_1 T_{22}^*)^2}}{\sqrt{(T_{21}^* - \omega^2 Z_1 Z_2 T_{12}^*)^2 + \omega^2 (Z_2 T_{11}^* + Z_1 T_{22}^*)^2}} = 0. \quad (26)$$

As a result, the full transmission conditions for the asymmetric system can be derived,

$$\begin{aligned} Z_2 T_{11}^* &= Z_1 T_{22}^*, \\ T_{21}^* + \omega^2 Z_1 Z_2 T_{12}^* &= 0. \end{aligned} \quad (27)$$

Substituting Eq. (27) into Eq. (24) and using the fact that $\det \mathbf{T}^* = 1$, the transmission coefficient can be rewritten as

$$\begin{aligned} T &= \frac{2\omega Z_1}{\omega(Z_2 T_{11}^* + Z_1 T_{22}^*) + i(\omega^2 Z_1 Z_2 T_{12}^* - T_{21}^*)} \\ &= \frac{2\omega Z_1}{2\omega Z_1 T_{22}^* + 2\omega Z_1 i(\omega Z_2 T_{12}^*)} \\ &= \frac{1}{T_{22}^* + i\omega Z_2 T_{12}^*} = \frac{T_{22}^* - i\omega Z_2 T_{12}^*}{T_{22}^{*2} + \omega^2 Z_2^2 T_{12}^{*2}} \\ &= \frac{Z_1}{Z_2} T_{22}^* - i\omega Z_1 T_{12}^* \\ &= T_{11}^* - i\omega Z_1 T_{12}^*. \end{aligned} \quad (28)$$

In Eq. (28), it can be seen that the transmission coefficient has both real and imaginary values, while in the symmetric system the transmission coefficient was purely imaginary so that only the phase shifts of $\pi/2$ or $3\pi/2$ were possible. From Eq. (28), the magnitude and phase shift can be

obtained as

$$|T| = \sqrt{T_{11}^{*2} + \omega^2 Z_1^2 T_{12}^{*2}} \\ = \sqrt{\frac{Z_1}{Z_2} T_{11}^* T_{22}^* + \omega^2 Z_1 Z_2 T_{12}^* \frac{Z_1}{Z_2} T_{12}^*} = \sqrt{\frac{Z_1}{Z_2}}, \quad (29)$$

$$\phi = \sin^{-1} \left(-\frac{\omega m_{\text{eff}}}{\sqrt{Z_1 Z_2}} \right). \quad (30)$$

Comparing Eqs. (29) and (30) with the previous results, the magnitude of the transmission coefficient is the same as in the previous symmetric case. This is obvious since both are calculated under the full transmission condition. However, unlike the previous symmetric case, various phase shifts can be derived by adjusting m_{eff} , as shown in Eq. (30). This indicates that the asymmetric system is not affected by the limitation and both the full transmission and the desired phase shifts can be achieved simultaneously.

Finally, these equations are rearranged to figure out the required effective parameters. To achieve the desired phase shift ϕ under full transmission, the effective parameters are derived as a function of the phase shift. From Eq. (28), the following equation is derived:

$$T = |T| \cos \phi + i |T| \sin \phi = T_{11}^* - i \omega Z_1 T_{12}^*. \quad (31)$$

From the imaginary value in Eq. (31), the effective mass is derived as

$$|T| \sin \phi = -\omega Z_1 T_{12}^* = \frac{T_{21}^*}{\omega Z_2} = \frac{-\omega m_{\text{eff}}}{Z_2}, \quad (32)$$

or simply,

$$m_{\text{eff}} = -\frac{\sqrt{Z_1 Z_2}}{\omega} \sin \phi. \quad (33)$$

Also, from the real value in Eq. (31), the following relationship can be derived:

$$|T| \cos \phi = T_{11}^* = \frac{\beta_{\text{eff}} - \omega^2 m_{\text{eff}}}{\beta_{\text{eff}}}, \quad (34)$$

$$\beta_{\text{eff}} = -\frac{\omega \sqrt{Z_1 Z_2}}{1 - \sqrt{(Z_1/Z_2)} \cos \phi} \sin \phi. \quad (35)$$

Furthermore, by using the full transmission condition in Eq. (27),

$$|T| \cos \phi = T_{11}^* = \frac{Z_1}{Z_2} T_{22}^* = \frac{Z_1 \alpha_{\text{eff}} - \omega^2 m_{\text{eff}}}{\alpha_{\text{eff}}}, \quad (36)$$

$$\alpha_{\text{eff}} = -\frac{\omega \sqrt{Z_1 Z_2}}{1 - \sqrt{(Z_2/Z_1)} \cos \phi} \sin \phi. \quad (37)$$

To manipulate waves with metasurfaces, various phase shifts ϕ from 0 to 2π are required. From Eqs. (32)–(37),

it can be seen that the effective parameters should also be varied from negative to positive values to achieve the phase shifts from 0 to 2π . In conclusion, if a metasurface unit is designed to have asymmetry and effective parameters varying from negative to positive values, wave manipulation between different mediums becomes possible.

In Eqs. (32)–(37), it can be seen that the effective parameters have singular points. For instance, if ϕ is 0 or π all effective parameters become zero, which is physically impossible. Also, if ϕ is a certain value satisfying $\cos \phi = \sqrt{Z_1/Z_2}$ (when $Z_2 > Z_1$), effective spring coefficients become infinite in value. Fortunately, this issue is easily avoided by replacing the singular phase shifts with slightly deviated values. For instance, the singular phase shifts $\phi = \pi$ can be realized with a small deviation of 0.013 rad, as will be shown in the numerical simulations in this paper.

It is worth noting that the idea of the asymmetric unit cell is in fact related to Willis coupling metamaterials.

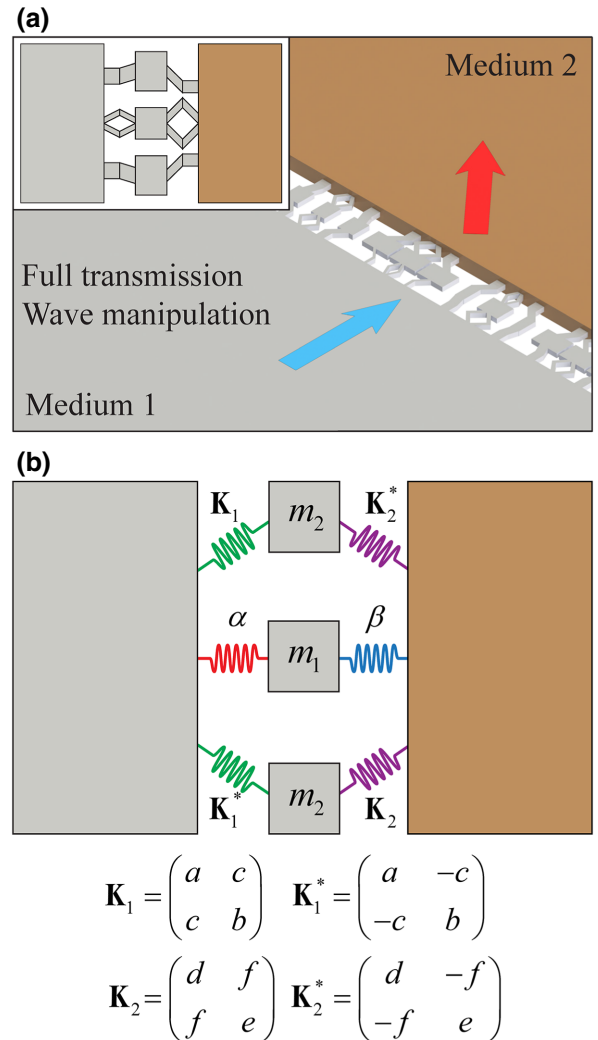


FIG. 4. Schematics of (a) the proposed asymmetric metasurface and (b) equivalent mass-spring system.

Willis coupling is induced from geometrical asymmetry, which causes changes in phenomena on the boundary. From Willis coupling, the diagonal components of the transfer matrix become different. Likewise, in this research, the asymmetric elastic couplings result in the difference between diagonal components of the transfer matrix. The difference in diagonal components changes the full transmission condition, so full transmission and the desired phase shift can be achieved simultaneously.

III. ACTUAL UNIT DESIGN FOR AN ASYMMETRIC METASURFACE

The theoretical investigations shown in the previous section are summarized as follows. First, to achieve wave manipulation between two different mediums, the metasurface should be equivalent to the asymmetric system consisting of two different equivalent springs. In addition, each unit should be properly designed so that its equivalent parameters vary from negative to positive values. To achieve these goals, the single-unit metasurface [20] is adopted and modified. As shown in Fig. 4(a), the metasurface unit consists of a horizontal resonator and a pair of vertical resonators. Under the incident longitudinal wave, the horizontal resonator is known to tune the effective mass from negative to positive values. On the other hand, the vertical resonator pair exhibits large vertical motion, providing an effective spring coefficient from negative to positive values [20]. In addition, each resonator in this research is designed asymmetrically to achieve the asymmetry, the key to wave manipulation between two different mediums.

To check whether the proposed metasurface unit is equivalent to the asymmetric system shown in Fig. 3, the

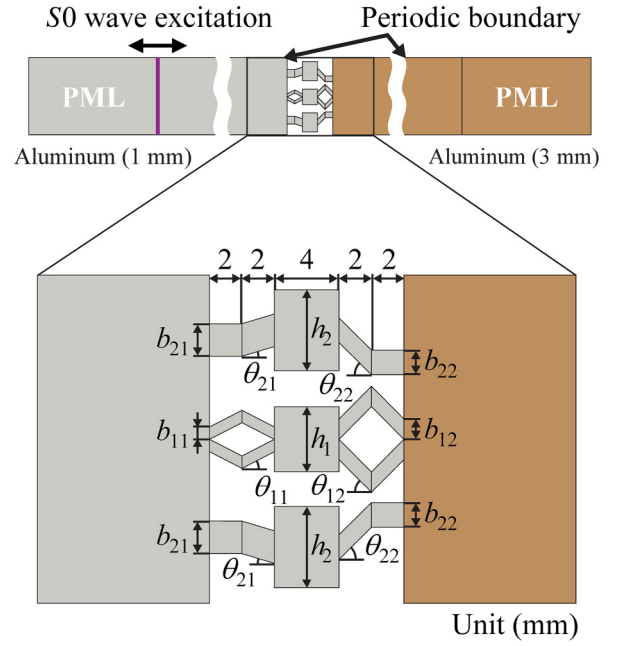


FIG. 5. Simulation setting used for the metasurface unit design with detailed geometry.

equivalent parameters are theoretically derived. To this end, the actual structure in Fig. 4(a) is converted to the mass-spring system shown in Fig. 4(b). Here, since the unit configuration is asymmetric, the springs on the left of the mass are different from the springs on the right of the mass in Fig. 4(b). Note that K_1, K_2, K_1^* , and K_2^* are the matrices containing the spring constants for each axis a, b, d, e , and the coupled spring constants c and f . From the mass-spring system shown in Fig. 4(b), the equation of motion for each mass is given as

$$\begin{aligned}
 -m_1\omega^2 u_1 &= \alpha(u_o - u_1) + \beta(u_d - u_1), \\
 -m_2\omega^2 u_2 &= a(u_o - u_2) + d(u_d - u_2) - (c - f)v_2, \\
 -m_2\omega^2 v_2 &= -(b + e)v_2 + c(u_o - u_2) - f(u_d - u_2), \\
 -m_2\omega^2 u_3 &= a(u_o - u_3) + d(u_d - u_3) + (c - f)v_3, \\
 -m_2\omega^2 v_3 &= -(b + e)v_3 - c(u_o - u_3) + f(u_d - u_3).
 \end{aligned} \tag{38}$$

From Eq. (38), u_1 is the horizontal displacement for mass m_1 , u_2 is the one for upper mass m_2 , and u_3 is the one for bottom mass m_2 . v is the vertical displacement for each mass. From these equations, each displacement is expressed in terms of u_o and u_d as follows:

$$\begin{aligned}
 u_1 &= \frac{\alpha u_o + \beta u_d}{\alpha + \beta - m_1\omega^2}, \\
 u_2 = u_3 &= \frac{(b + e - m_2\omega^2)(a u_o + d u_d) - (c - f)(c u_o - f u_d)}{(a + d - m_2\omega^2)[(b + e - m_2\omega^2) - (c - f)^2]}, \\
 v_2 = -v_3 &= \frac{(a + d - m_2\omega^2)(c u_o - f u_d) - (c - f)(a u_o + d u_d)}{(a + d - m_2\omega^2)[(b + e - m_2\omega^2) - (c - f)^2]}.
 \end{aligned} \tag{39}$$

On the other hand, from the equations of motion, the boundary forces at $x = 0$ and $x = d$ are derived as

$$\begin{aligned} f_o &= \alpha(u_1 - u_o) + a(u_2 - u_o) + a(u_3 - u_o) + 2cv_2 = \alpha u_1 + 2au_2 + 2cv_2 - (\alpha + 2a)u_o, \\ f_d &= \beta(u_d - u_1) + d(u_d - u_2) + d(u_d - u_3) + 2f v_2 = -\beta u_1 - 2du_2 + 2f v_2 + (\beta + 2d)u_d. \end{aligned} \quad (40)$$

Substituting Eq. (39) into Eq. (40), the boundary forces are derived in terms of u_o and u_d ,

$$\begin{aligned} f_o &= X_1 u_o + X_3 u_d, \\ f_d &= -X_3 u_o - X_2 u_d, \end{aligned} \quad (41)$$

where

$$\begin{aligned} X_1 &= \frac{\alpha^2}{\alpha + \beta - m_1 \omega^2} + \frac{2[a^2(b + e - m_2 \omega^2) + c^2(a + d - m_2 \omega^2) - 2ac(c - f)]}{(a + d - m_2 \omega^2)(b + e - m_2 \omega^2) - (c - f)^2} - (\alpha + 2a), \\ X_2 &= \frac{\beta^2}{\alpha + \beta - m_1 \omega^2} + \frac{2[d^2(b + e - m_2 \omega^2) + f^2(a + d - m_2 \omega^2) - 2df(c - f)]}{(a + d - m_2 \omega^2)(b + e - m_2 \omega^2) - (c - f)^2} - (\beta + 2d), \\ X_3 &= \frac{\alpha\beta}{\alpha + \beta - m_1 \omega^2} + \frac{2[ad(b + e - m_2 \omega^2) - cf(a + d - m_2 \omega^2) + (af - cd)(c - f)]}{(a + d - m_2 \omega^2)(b + e - m_2 \omega^2) - (c - f)^2}. \end{aligned} \quad (42)$$

As a result, the transfer matrix of the equivalent system can be described as

$$T^* = \frac{1}{X_3} \begin{pmatrix} -X_1 & 1 \\ X_1 X_2 - X_3^2 & -X_2 \end{pmatrix}. \quad (43)$$

From Eq. (43), the effective parameters are derived by using the relationship between the elements of the transfer matrix and the effective parameters derived from the correspondence to Eq. (23),

$$\begin{aligned} T_{21}^* &= -\omega^2 m_{\text{eff}} = \frac{X_1 X_2 - X_3^2}{X_3}, & m_{\text{eff}} &= -\frac{X_1 X_2 - X_3^2}{\omega^2 X_3}, \\ T_{22}^* &= \frac{\alpha_{\text{eff}} - \omega^2 m_{\text{eff}}}{\alpha_{\text{eff}}} = -\frac{X_2}{X_3}, & \alpha_{\text{eff}} &= -\frac{X_1 X_2 - X_3^2}{X_2 + X_3}, \\ T_{11}^* &= \frac{\beta_{\text{eff}} - \omega^2 m_{\text{eff}}}{\beta_{\text{eff}}} = -\frac{X_1}{X_3}, & \beta_{\text{eff}} &= -\frac{X_1 X_2 - X_3^2}{X_1 + X_3}. \end{aligned} \quad (44)$$

In Eq. (44), it can be seen that α_{eff} is not same as β_{eff} . This indicates that the asymmetric unit shown in Fig. 4(a) is equivalent to the asymmetric mass-spring system shown in Fig. 3. Also, from Eq. (42), it can be seen that the denominators in X_1 , X_2 , and X_3 have zero values around the resonance frequencies of the horizontal or vertical resonators, $\omega = (\alpha + \beta)/m_1$, $(a + d)/m_2$, or $(b + e)/m_2$, indicating that X_1 , X_2 , and X_3 may vary from negative to positive values. Accordingly, the effective parameters in Eq. (44) are also tunable from negative to positive values. In conclusion, the theoretical results in Eq. (44) show that the two requirements, the asymmetry and the tunability from negative to positive values, are satisfied with the proposed asymmetric metasurface unit. Thus, with the asymmetric

TABLE I. Actual design parameters for units of the proposed asymmetric metasurface, which are described in Fig. 5.

Unit	Design parameters									
	h_1 (mm)	h_2 (mm)	b_{11} (mm)	b_{12} (mm)	θ_{11} (deg)	θ_{12} (deg)	b_{21} (mm)	b_{22} (mm)	θ_{21} (deg)	θ_{22} (deg)
1	6.000	2.345	1.057	5.000	30.39	40.00	2.000	1.305	2.09	44.10
2	2.933	3.782	5.000	1.181	44.76	45.00	2.000	2.000	44.05	0.57
3	5.166	2.224	1.480	7.515	44.69	43.77	1.931	1.103	25.50	45.00
4	3.140	3.596	7.168	7.871	38.70	34.73	1.779	1.992	43.41	19.70
5	5.995	6.000	5.522	1.281	24.17	43.71	6.268	1.918	41.94	44.90
6	4.736	2.100	9.977	6.337	43.67	25.05	1.976	1.943	15.44	44.13
7	4.704	5.945	9.561	8.818	42.42	34.47	1.149	1.306	28.97	19.62
8	3.083	2.383	1.081	9.200	42.17	43.98	1.326	1.666	28.48	23.97

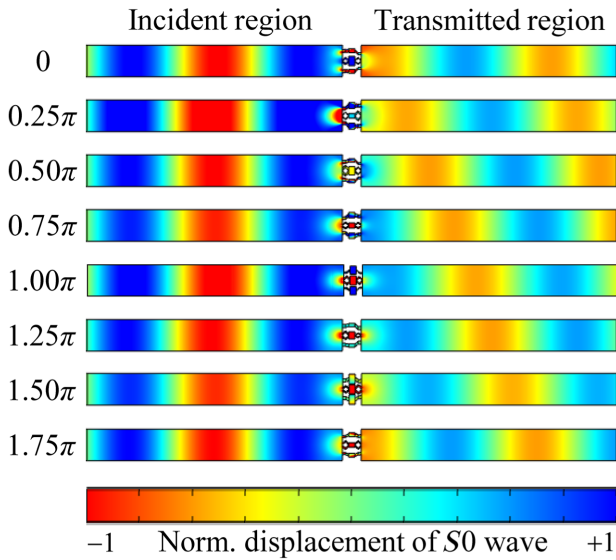


FIG. 6. Results of numerical simulation for each designed metasurface unit.

units, wave manipulation between two different mediums is possible.

IV. NUMERICAL VALIDATIONS

To validate whether the proposed metasurface unit can manipulate wave between two different mediums, several wave manipulation examples are numerically investigated. Here, aluminum plates with thicknesses of 1 and 3 mm are considered as the different wave mediums. Note that although the material properties are same, the wave impedance is different if the thicknesses of the plates are different, as shown in Ref. [19]. In all simulations, the longitudinal wave (more specifically, the lowest-order symmetric Rayleigh-Lamb wave mode [26]) with the frequency of 50 kHz is considered.

First, wave steering, which redirects the transmitted wave along the desired angle, is considered. To achieve

TABLE II. Transmission coefficient and phase shift for each unit cell: $T_{ideal} = 0.5774$.

Objective phase shift ϕ_{ideal} (rad)	Designed phase shift ϕ (rad)	Designed transmission T/T_{ideal}
0	-0.0447π	0.9927
0.25π	0.2623π	0.9960
0.50π	0.5280π	0.9997
0.75π	0.8094π	0.9952
1.00π	0.9598π	0.9998
1.25π	1.2504π	0.9958
1.50π	1.4989π	0.9990
1.75π	1.7809π	0.9991

wave steering, eight metasurface units are considered to achieve the phase shift at every $\pi/4$ from 0 to 2π rad (the corresponding phase gradient is 12.5π rad/m). Figure 5 plots the simulation setting to design the asymmetric metasurface units with the desired phase shifts with full transmission. To design actual continuum units corresponding to the desired phase shifts, the following design variables are chosen: the height of each mass, h_1 and h_2 , and the variables to change the beam of each resonator, b_{11} , b_{12} , b_{21} , b_{22} , θ_{11} , θ_{12} , θ_{21} , and θ_{22} in Fig. 5. In the metasurface unit design, one may use Eqs. (42) and (44), but it is extremely complicated and inaccurate to use the theoretical equations due to the continuum nature. Thus, we adopt the well-known particle swarm optimization (PSO) algorithm [27] to achieve the desired design variables. The PSO algorithm is one of the most widely used heuristic and iterative optimization methods, and it has advantages in solving complex problems. In the PSO algorithm, a set of design variables is considered as a particle that has its own velocity and inertia. Initially, particles are randomly distributed throughout the design space that is spanned by design variables. For each particle, the calculation of an objective function is carried out, and the lowest value of the function among the particles becomes a personal best,

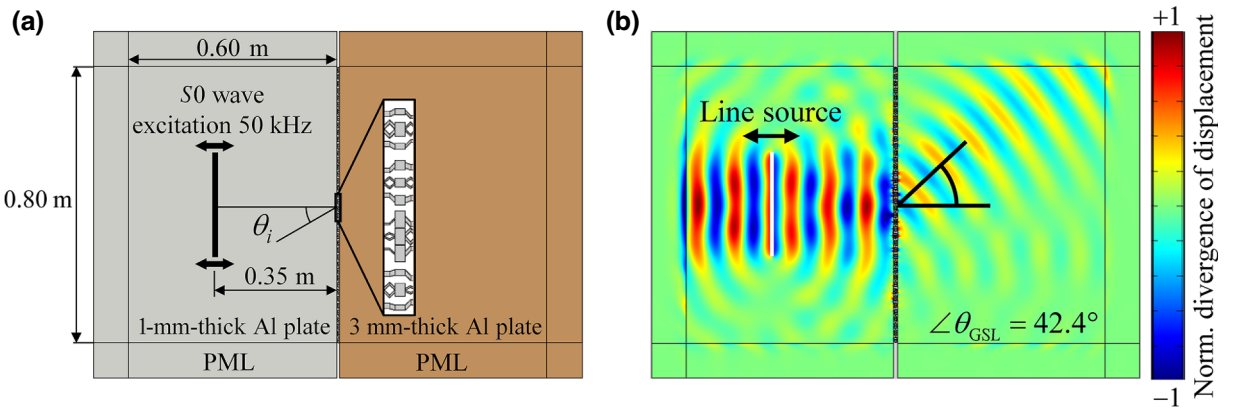


FIG. 7. (a) Simulation setting for the wave-steering metasurface and (b) longitudinal wave plot as the simulation result.

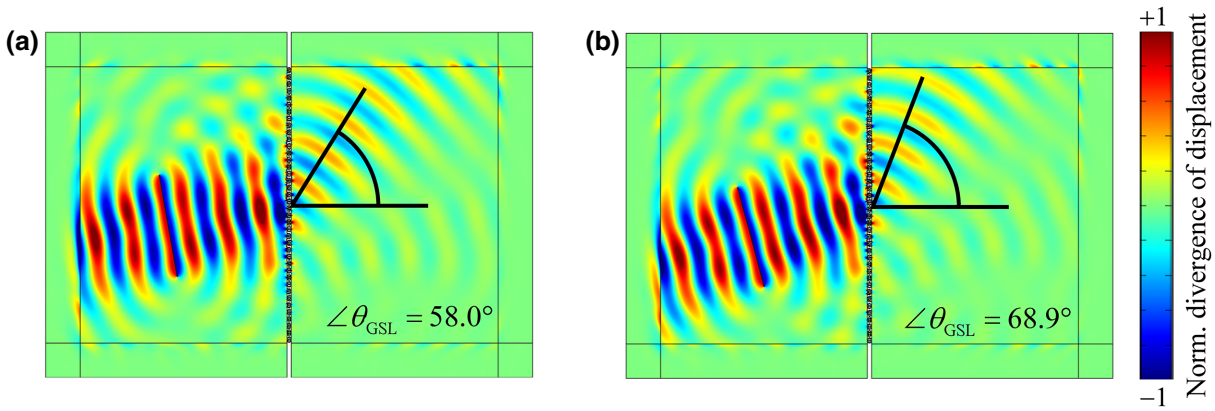


FIG. 8. Results of numerical simulation with the incident angles of (a) 10°, (b) 15°.

which also becomes a global best value and location. In the next iteration, the locations of each particle are randomly updated based on their own velocity and inertia. Then, the value of the function at each updated location is calculated again, and a personal best is determined again. At that time, if the personal best value is smaller than the global value, the global value is replaced with the personal best value, and if not, the global best is maintained. Through iterations, the global best approaches the best solution, which provides the desired metasurface unit design. As a result of the PSO algorithm, the designed variables for the desired phase shift and almost full transmission are summarized in Table I. Also, the numerical results of each unit of the metasurface are shown in Fig. 6, and the resulting transmission coefficients and phase shifts are listed in Table II. The largest error in the transmission coefficients is smaller than 1% ($T_{\min} = 0.993T_{\text{ideal}}$), and the largest error in phase shifts is smaller than 8%.

Based on the designed metasurface units, actual wave simulations are performed. The simulation setting is shown in Fig. 7(a). Here, 40 metasurface units are placed between two $0.6 \times 0.8 \text{ m}^2$ aluminum plates with thicknesses of 1

and 3 mm. To eliminate any undesired reflections, a perfectly matched layer (PML) is placed around the plates. A 0.3-m-long S_0 wave line source is placed in the 1-mm-thick aluminum plate. Figure 7(b) plots the wave simulation result. As can be seen in Fig. 7(b), the normally incident longitudinal wave is successfully refracted as desired. The numerically calculated refraction angle is 42.0° , which agrees well with the theoretically predicted angle of 42.4° from the generalized Snell’s law. Also, in Fig. 7(b), the wave displacements at the left and right sides of the wave source are almost the same, indicating that there is almost no reflection from the metasurface. As a result, it is validated that the proposed asymmetric metasurface can manipulate waves with full transmission between two different mediums, which was impossible with the previous approaches.

To check whether the proposed asymmetric metasurface is still valid in the obliquely incident case, numerical simulations are repeated with various incident angles. Figures 8 and 9 plot various wave simulation results with the various incident angles. Note that if the incident angle becomes larger than 19° , wave steering is no longer possible since

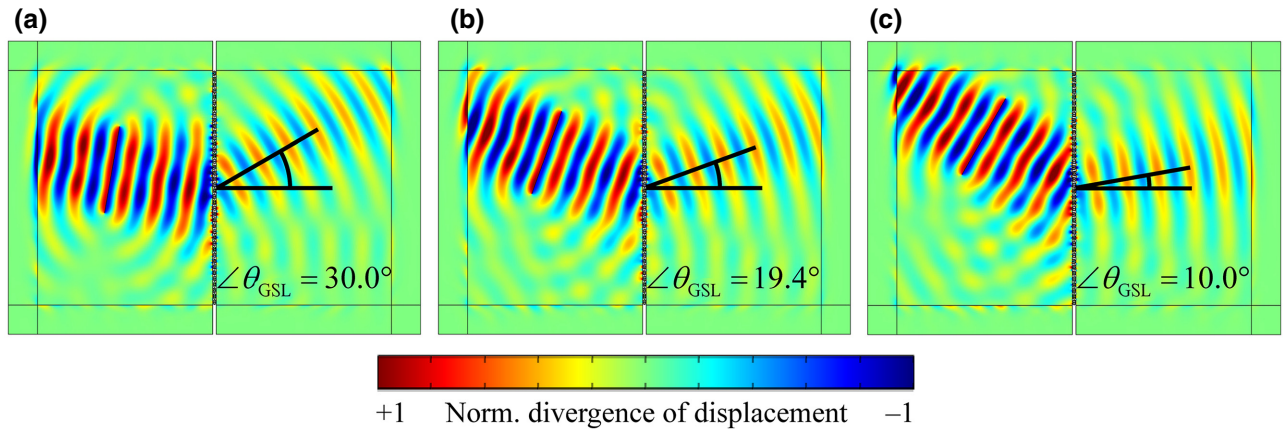


FIG. 9. Results of numerical simulation with the incident angles of (a) -10° , (b) -20° , (c) -30° , respectively.

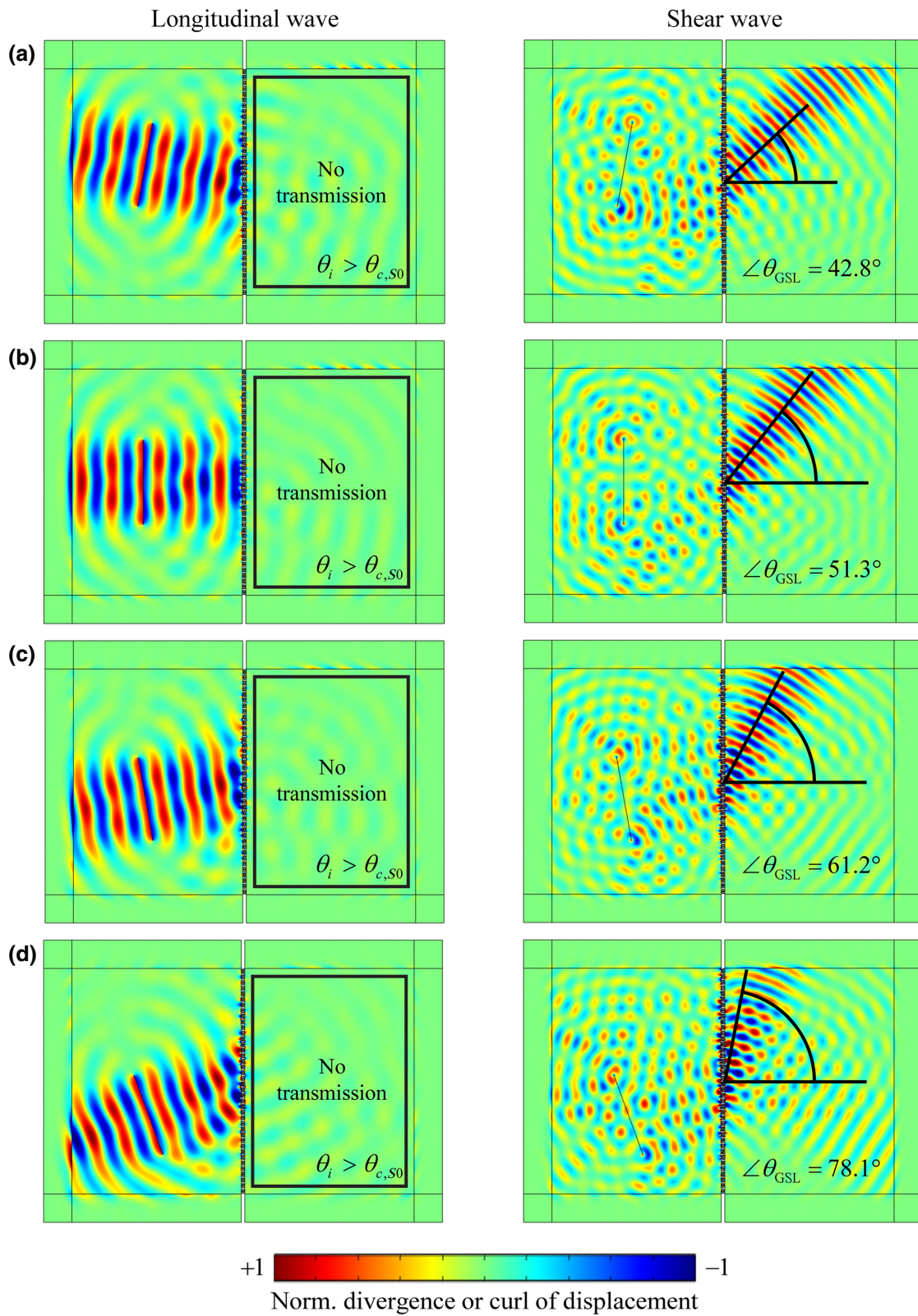


FIG. 10. Results of numerical simulation for the transmodal metasurface with the incident angles of (a) -10° , (b) 0° , (c) 10° , (d) 20° , respectively.

a surface wave is formed and diffraction dominates. As can be seen in Figs. 8 and 9, although the metasurface is designed under the normally incident wave, wave steering is still possible for the obliquely incident case. Also, it can be clearly seen that there is almost no reflection from the metasurface. The numerically calculated refraction angles are 11.8° , 20.4° , 30.4° , 55.2° , and 65.8° for incident angles of -30° , -20° , -10° , 10° , and 15° , which agree well with the theoretical generalized Snell's law predictions of 10.0° , 19.4° , 30.0° , 58.0° , and 68.9° , respectively. From the simulation results, it can be seen that the wave manipulation between two different mediums is sufficiently robust that it can cover a broad range of incident angles.

To further validate the proposed metasurface, other applications are also investigated. First, the transmodal metasurface [13,28], which fully converts the incident longitudinal wave into the refracted shear wave is studied. In previous studies, it was shown that if the metasurface is designed to have a very large phase gradient so that the refracted longitudinal wave becomes a surface wave while the refracted shear wave forms a propagating wave, the incident longitudinal wave is totally converted to a shear wave for various incident angles. To achieve the transmodal metasurface between two different mediums, the metasurface units in Table I are reconsidered. However, only the metasurface units for the phase shifts of 0.25π , 0.75π , 1.25π , and 1.75π rad are chosen to double the phase gradient as 25 rad/m. With this large phase gradient, the transmodal metasurface is expected to operate for incident angles from -20.4° to 22.3° . To check whether the transmodal metasurface is achieved between two different mediums, the wave simulation in Fig. 7(a) is repeated with the four units and the various incident angles of -10° , 0 , 10° , and 20° .

Figure 10 plots the wave simulation results. Note that the same simulation results are plotted twice in Fig. 10—one for the longitudinal wave only and the other for the shear wave only. From the left-hand figures in Fig. 10 (where

only the longitudinal wave is plotted), it can be seen that only the incident waves are plotted. This indicates that there are almost no reflected or refracted longitudinal waves. On the other hand, the shear wave plot in Fig. 10 shows that shear waves are refracted with angles of 43.2° , 51.1° , 60.8° , and 73.9° , which are almost same as the theoretical predictions of 42.8° , 51.3° , 61.2° , and 78.1° , respectively. As a result, it can be concluded that the incident longitudinal wave is almost converted to a refracted shear wave, with almost no reflection. It is worth emphasizing that, according to classical elastic wave theory, such total mode conversion is only possible along a certain incident angle, while the designed transmodal metasurface provides total mode conversion for a broad range of incident angles.

Next, let us consider beam focusing [17,18] between two different mediums. To achieve beam focusing, the following phase shifts are required:

$$\phi = k_t \left(\sqrt{l^2 + y^2} - l \right), \quad (45)$$

where k_t is the wave number in the transmitted region and l is the desired focal length, which is set to be 0.15 m. Here, we repeat the PSO-based design to fit the desired phase shifts with full transmission. Figure 11(a) plots the required phase shifts (red line) and the designed phase shifts (blue circles) achieved by the PSO algorithm. Note that the minimum transmission for all designed units is 0.573 ($= 0.99 T_{\text{ideal}}$), indicating that almost full transmission is also achieved. Figure 11(b) is the numerical simulation of the beam focusing between two different mediums. Here, the simulation setting is same as in Fig. 7(a), while the metasurface units are replaced with the redesigned units. Also, to ensure plane-wave incidence, the longitudinal line source is enlarged to 0.8 m. As can be clearly seen in Fig. 11(b), the longitudinal wave is well focused around the expected focal point located at 0.15 m from

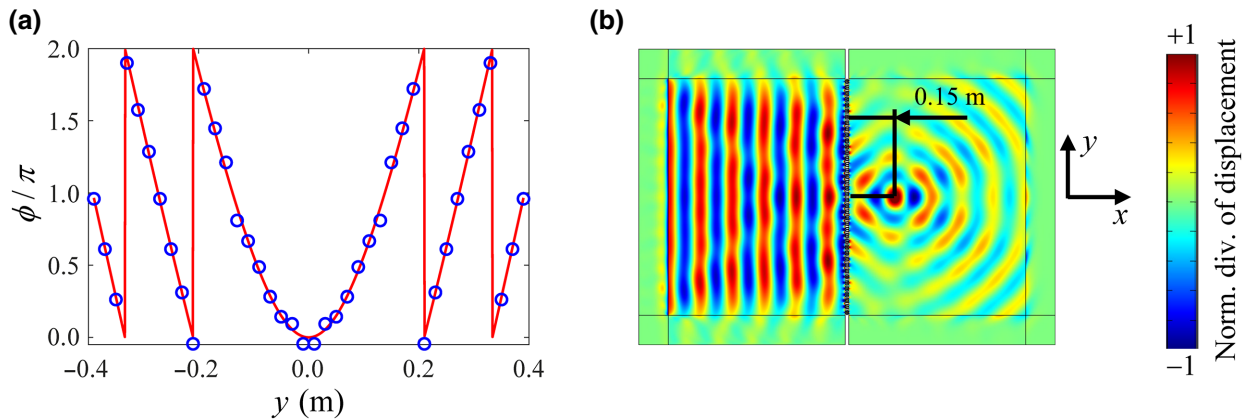


FIG. 11. (a) The phase profile and (b) numerical simulation result of the wave-focusing metasurface.

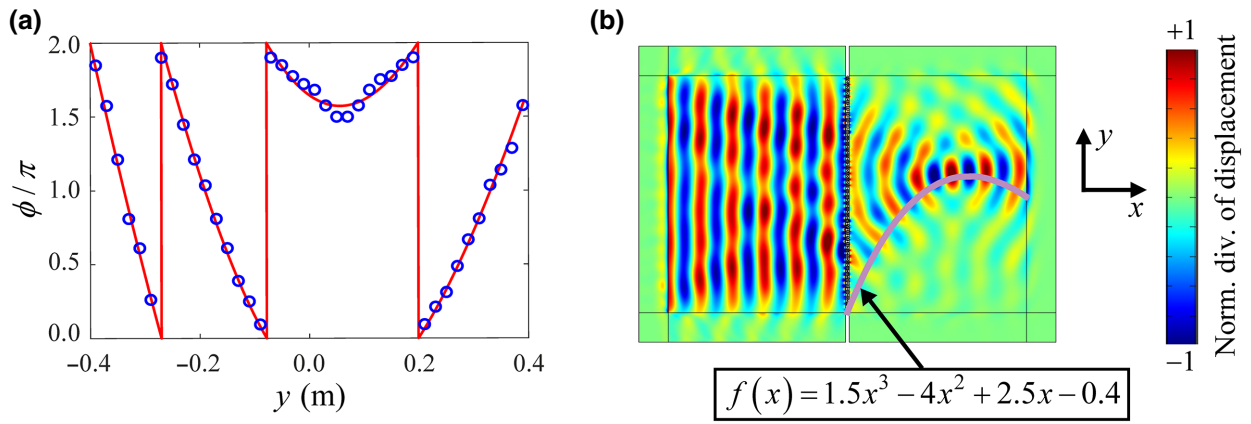


FIG. 12. (a) The phase profile and (b) numerical simulation result of the self-bending beam with the proposed metasurface.

the metasurface, validating that the beam focusing between two different mediums is achieved.

Finally, the self-bending beam [17,29,30] between two different mediums is considered. The self-bending beam indicates that the transmitted waves are guided along the desired trajectory. The phase shifts required to achieve the self-bending beam is calculated by the Legendre transform method [17,30]. Here, the following curve is considered as the desired trajectory, and the phase shifts are calculated based on it:

$$f(x) = 1.5x^3 - 4x^2 + 2.5x - 0.4. \quad (46)$$

The red line in Fig. 12(a) plots the required phase shifts to achieve the self-bending beam with the desired trajectory. Again, the phase shifts are achieved by the PSO algorithm. The achieved phase shifts, with the minimum transmission of 0.560 ($= 0.97 T_{\text{ideal}}$), are plotted as the blue circles in Fig. 12(a). The wave simulation result is plotted in Fig. 12(b). The simulation setting is set to be same as in Fig. 11(b), except that the metasurface is replaced by the redesigned units. Figure 12(b) clearly shows that the transmitted waves propagate along the desired trajectory, plotted as the solid purple line. The simulation results in Figs. 11(b) and 12(b) strongly support that various wave manipulations between two different mediums are possible with the proposed asymmetric metasurface.

V. CONCLUSION

In this paper, the asymmetric metasurface is proposed as a means of wave manipulation between two different mediums. Although there have been various studies on metasurfaces, the homogeneous case where the wave medium is same before and after the metasurface has usually been studied. Here, we theoretically show that these previous approaches for the homogeneous case have a limitation in that they cannot be applied to the inhomogeneous

case where the metasurface is placed between two different mediums. It is shown that it is impossible to achieve both full transmission and desired phase shifts between two different mediums simultaneously if the general mass-spring system is considered. However, we find that by introducing asymmetry, one can break through the limitation and achieve both full transmission and the desired phase shifts even when the metasurface is between two different mediums. In other words, wave manipulation between two different mediums is possible if asymmetry is introduced into the metasurface. This becomes possible due to the difference in the diagonal components of the transfer matrix. From geometrical asymmetry, the difference in diagonal terms occurs and changes the full transmission condition. As a result, various phase shifts for wave manipulation become achievable. To realize the asymmetry, we propose an asymmetric metasurface consisting of asymmetric horizontal and vertical resonators. With the proposed metasurface, wave steering between two different mediums is numerically investigated. Owing to the asymmetry, wave steering is successfully achieved, which was impossible with the previous approaches. In addition, various wave manipulations, such as total mode conversion, beam focusing, and self-bending beam, are successfully achieved between two different mediums.

The main achievement of the paper is summarized as follows. First, we present the metasurface enabling wave manipulation between two different mediums. Previous research on wave manipulation by acoustic and elastic metasurfaces were only valid for the case where the metasurface is located between identical mediums. Furthermore, recently it was shown that it is theoretically impossible to apply the previous research to a metasurface between different mediums. In contrast, this research presents a way to solve this theoretical limitation. Also, this paper provides a possible connection between the two different fields of metasurfaces and Willis coupling. As mentioned, the idea of asymmetry is in fact deeply related

to Willis coupling. We show that Willis coupling (the geometric asymmetry) enables the metasurface between two different mediums. In addition, as shown in the various examples, current research is expected to open the field of metasurfaces for the inhomogeneous case. Considering that most of the engineering applications of elastic waves involve multiple materials, our asymmetric metasurface can provide opportunities in various applications such as nondestructive evaluation or medical ultrasonic applications where waves are transmitted between different mediums.

Finally, it is worth mentioning that although our research mainly considers longitudinal waves, the same idea holds for shear waves or acoustic cases owing to their physical similarities. However, current research has a limitation in that it cannot be applied to the flexural wave case. As shown in previous research, flexural waves are largely affected by evanescent waves. For instance, it was shown that evanescent waves in the metasurface unit cell largely affect the transmission phenomena so that very high transmission is achievable [31]. In the same manner, there is a possibility that the evanescent wave provides another solution for the wave manipulation between two different mediums. We would like to leave this topic for any possible future work here.

ACKNOWLEDGMENTS

This work was supported by the Center for Advanced Meta-Materials (CAMM) funded by the Ministry of Science, ICT and Future Planning as Global Frontier Project (Project No. CAMM-2014M3A6B3063711), by the National Research Foundation of Korea (NRF) grants funded by the Korean government (Grants No. 2020R1A2C4002383 and No. 2021R1A4A1033224). The authors thank Mr. Chan Wook Park and Professor Yoon Young Kim of Seoul National University for their valuable comments during the research.

-
- [1] N. Yu, P. Genevet, M. A. Kats, F. Aieta, J. P. Tetienne, F. Capasso, and Z. Gaburro, Light propagation with phase discontinuities: Generalized laws of reflection and refraction, *Science* **334**, 333 (2011).
- [2] F. Monticone, N. M. Estakhri, and A. Alù, Full Control of Nanoscale Optical Transmission with a Composite Metascreen, *Phys. Rev. Lett.* **110**, 203903 (2013).
- [3] X. Ni, A. V. Kildishev, and V. M. Shalaev, Metasurface holograms for visible light, *Nat. Commun.* **4**, 2807 (2013).
- [4] P. Y. Chen, J. Soric, Y. R. Padooru, H. M. Bernety, A. B. Yakovlev, and A. Alù, Nanostructured graphene metasurface for tunable terahertz cloaking, *New J. Phys.* **15**, 123029 (2013).
- [5] H. Chu, H. Zhang, Y. Zhang, R. Peng, M. Wang, Y. Hao, and Y. Lai, Invisible surfaces enabled by the coalescence of anti-reflection and wavefront controllability in ultrathin metasurfaces, *Nat. Commun.* **12**, 4523 (2021).
- [6] W. Lee, S. Jo, K. Lee, H. S. Park, J. Yang, H. Y. Hong, C. Park, S. K. Hong, and H. Lee, Single-layer phase gradient mmWave metasurface for incident angle independent focusing, *Sci. Rep.* **11**, 12671 (2021).
- [7] Y. Xie, W. Wang, H. Chen, A. Konneker, B. I. Popa, and S. A. Cummer, Wavefront modulation and subwavelength diffractive acoustics with an acoustic metasurface, *Nat. Commun.* **5**, 5553 (2014).
- [8] B. Liu, W. Zhao, and Y. Jiang, Apparent negative reflection with the gradient acoustic metasurface by integrating supercell periodicity into the generalized law of reflection, *Sci. Rep.* **6**, 38314 (2016).
- [9] Y. Yang, H. Wang, F. Yu, Z. Xu, and H. Chen, A metasurface carpet cloak for electromagnetic, acoustic and water waves, *Sci. Rep.* **6**, 20219 (2016).
- [10] B. Liu, J. Zhao, X. Xu, W. Zhao, and Y. Jiang, All-angle negative reflection with an ultrathin acoustic gradient metasurface: Floquet-Bloch modes perspective and experimental verification, *Sci. Rep.* **7**, 13852 (2017).
- [11] S. W. Fan, Y. Zhu, L. Cao, Y. F. Wang, A. L. Chen, A. Merkel, Y. S. Wang, and B. Assouar, Broadband tunable lossy metasurface with independent amplitude and phase modulations for acoustic holography, *Smart Mater. Struct.* **29**, 105038 (2020).
- [12] L. Cao, Z. Yang, Y. Xu, and B. Assouar, Deflecting flexural wave with high transmission by using pillared elastic metasurface, *Smart Mater. Struct.* **27**, 075051 (2018).
- [13] M. S. Kim, W. R. Lee, Y. Y. Kim, and J. H. Oh, Transmodal elastic metasurface for broad angle total mode conversion, *Appl. Phys. Lett.* **112**, 241905 (2018).
- [14] Y. Jin, W. Wang, A. Khelif, and B. Djafari-Rouhani, Elastic Metasurfaces for Deep and Robust Subwavelength Focusing and Imaging, *Phys. Rev. Appl.* **15**, 024005 (2021).
- [15] X. S. Li, Y. F. Wang, and Y. S. Wang, Sparse binary metasurfaces for steering the flexural waves, *Extrem Mech. Lett.* **52**, 101675 (2022).
- [16] Y. Hu, Y. Zhang, G. Su, M. Zhao, B. Li, Y. Liu, and Z. Li, Realization of ultrathin waveguides by elastic metagratings, *Commun. Phys.* **5**, 62 (2022).
- [17] Z. Lin and S. Tol, Elastic metasurfaces for full wavefront control and low-frequency energy harvesting, *J. Vib. Acoust.* **143**, 061005 (2021).
- [18] Y. Shen, Y. Xu, F. Liu, F. Wang, and Z. Yang, 3D-printed meta-slab for focusing flexural waves in broadband, *Extrem Mech. Lett.* **48**, 101410 (2021).
- [19] S. W. Lee, Y. J. Shin, H. W. Park, H. M. Seung, and J. H. Oh, Full-wave Tailoring Between Different Elastic Media: A Double-Unit Elastic Metasurface, *Phys. Rev. Appl.* **16**, 064013 (2021).
- [20] S. W. Lee and J. H. Oh, Single-layer elastic metasurface with double negativity for anomalous refraction, *J. Phys. D: Appl. Phys.* **53**, 265301 (2020).
- [21] T. G. Álvarez-Arenas, Acoustic impedance matching of piezoelectric transducers to the air, *IEEE Trans. Ultrason. Ferroelectr. Freq. Control* **51**, 624 (2004).
- [22] Y. Wang, K. Deng, S. Xu, C. Qiu, H. Yang, and Z. Liu, Applications of antireflection coatings in sonic crystal-based acoustic devices, *Phys. Lett. A* **375**, 1348 (2011).

- [23] Y. Duan, J. Luo, G. Wang, Z. H. Hang, B. Hou, J. Li, P. Sheng, and Y. Lai, Theoretical requirements for broadband perfect absorption of acoustic waves by ultra-thin elastic meta-films, *Sci. Rep.* **5**, 12139 (2015).
- [24] P. Markoš and C. M. Soukoulis, *Wave Propagation: From Electrons to Photonic Crystals and Left-Handed Materials* (Princeton University Press, Princeton, 2008).
- [25] H. Lee, J. K. Lee, H. M. Seung, and Y. Y. Kim, Mass-stiffness substructuring of an elastic metasurface for full transmission beam steering, *J. Mech. Phys. Solids* **112**, 577 (2018).
- [26] K. F. Graff, *Wave Motion in Elastic Solids* (Dover, Mineola, 1975).
- [27] J. Kennedy and R. Eberhart, in *Proc. IEEE Int. Conf. Neural Netw.* (1995), Vol. 4, pp. 1942.
- [28] M. Zheng, C. I. Park, X. Liu, R. Zhu, G. Hu, and Y. Y. Kim, Non-resonant metasurface for broadband elastic wave mode splitting, *Appl. Phys. Lett.* **116**, 171903 (2020).
- [29] P. Zhang, T. Li, J. Zhu, X. Zhu, S. Yang, Y. Wang, X. Yin, and X. Zhang, Generation of acoustic self-bending and bottle beams by phase engineering, *Nat. Commun.* **5**, 4316 (2014).
- [30] W. Wang, Y. Xie, B. I. Popa, and S. A. Cummer, Subwavelength diffractive acoustics and wavefront manipulation with a reflective acoustic metasurface, *J. Appl. Phys.* **120**, 195103 (2016).
- [31] Y. Liu, Z. Liang, F. Liu, O. Diba, A. Lamb, and J. Li, Source Illusion Devices for Flexural Lamb Waves Using Elastic Metasurfaces, *Phys. Rev. Lett.* **119**, 034301 (2017).